Soft Matter

PAPER

Length dependence of crosslinker induced network formation of rods: a Monte Carlo study

Raghunath Chelakkot[a] and Thomas Gruhn[*b]

Self-assembling filament networks are of great relevance for the development of novel materials. They show interesting mechanical properties and have exceptionally large internal surface areas. We analyzed the percolation behavior of a self-assembling network of rigid filaments and crosslinkers with the help of Monte Carlo simulations. In the system, filaments are represented by long spherocylinders, while crosslinkers are mimicked by short spherocylinders with adhesive sites at both ends with which the crosslinkers can bind to the filaments. We had analyzed the dependence of the network structure on the filament volume fraction, the crosslinker–filament ratio, and the adhesion strength in a former article (*Soft Matter*, 2009, **5**, 1504). In this work, we study the influence of the filament length on the percolation threshold, finding that, for a given filament volume fraction and crosslinker filament ratio, the percolation transition is rather independent of the filament length. We introduce an analytic approach, which reproduces the binding probability qualitatively.

1 Introduction

Scaffold-like supramolecular structures are remarkable in many aspects. Consisting of interconnected stiff or semiflexible filaments they may form a flexible network. Since the scaffold-like structure has a very large surface ratio, it is perfectly suited for high efficiency catalysts and molecular sensors.[1–9] In nanodevices, they may also be used as transistors or nanocircuits.[7,8,10–14] For these applications, the percolation behavior is of great relevance.[8,10,11] The electrical percolation in a mixture of carbon nanotubes and spherical latex particles has been studied in detail with the help of experiments, analytic calculations, and Monte Carlo simulations, showing that the percolation threshold can be finely controlled by the latex particle concentration.[11] Depending on the rigidity of the filaments and the strength of the bonds, the filament network may vary from being very flexible to very stable.[15–17] Together with the solvent the scaffold-like structures may form a bicontinuous phase, in which fluid and a filament path span the whole volume.

In cell biology, filament networks are found in the cytoskeleton. One part of the cytoskeleton that has been studied in much detail is the actin network, in which F-actin filaments are interconnected by crosslinkers like myosin, α-actinin and others.[18] This way, molecules may diffuse passively between the filaments or may be transported by molecular motors along the pathways of the actin network.[19–22] Furthermore, the filaments of the cytoskeleton stabilize the cell shape.[23,24] In the presence of ATP,

the actin network is a dynamic non-equilibrium system.[23,25] Filament growth and shrinking together with active crosslinking proteins make the cytoskeleton an extremely complex entity that can actively rearrange and thereby deform the cell and push it in a specific direction.[26–28] The mechanical behavior of the actin network is already of great interest in the passivated state and has been studied *in vitro* by many groups.[29–35] Various simulations of active[36–38] and passive networks[39,40,43,44] of stiff or semiflexible networks have been performed. A focus of these simulations is on rheological properties of the network under shear.[38,45–50]

While some quantitative results have been obtained for the mechanical properties, quantitative results of the structure and its dependence on system parameters are sparse. Recently, we have presented simulation results for a simple model system, which includes the essential aspects of crosslinker-mediated network formation.[42] The filaments are represented by long hard spherocylinders while crosslinkers are represented by short hard spherocylinders, which have adhesive sites on both ends. These sites can bind reversibly to the long spherocylinders. This model includes the essential components for the formation of a flexible scaffold-like network. The model is restricted to a small number of parameters. The structure of the system was studied systematically as a function of the filament volume fraction Φ, the crosslinker–filament ratio n_{lf}, and the strength of the bonds ε over the temperature T. Depending on these quantities, the filaments may either form isolated clusters or a room-spanning network. For a given length of the filament rods l_F, we determined the percolation threshold between the two phases as a function of the parameters Φ, n_{lr}, and ε. In this work, we extend this study by investigating the dependence of the percolation threshold on the filament rod lengths.

[a]*Martin Fisher School of Physics, Brandeis University, Waltham, MA-02454, USA*
[b]*Materials and Process Simulation (MPS), University of Bayreuth, Bayreuth, Germany. E-mail: Thomas.Gruhn@uni-bayreuth.de*

Actin filaments have a diameter of about $D \approx$ 7–9 nm, depending on the osmotic conditions.[51] *In vivo*, the filaments have a length of $l_F = 0.1$–1 μm so that $l_F/D \simeq 10$–120 (ref. 52). *In vitro*, actin filaments can polymerize to lengths up to 50 μm in the presence of divalent salt and ATP.[53] Frequently, capping proteins like CapZ are added which allows creating filaments with lengths typically found in cells.[54] In experiments, usual filament concentrations are in the range of 0.5–20 mg ml^{-1}, roughly corresponding to filament packing fractions in the range of $0.0015 < \Phi < 0.06$ (ref. 55). There are various types of actin-crosslinking proteins with various binding strengths ε. For example, at room temperature one has binding strengths $\varepsilon = 2T$ for α-actinin and $\varepsilon = 15T$ for fascin.[56] Here and in the following, the temperature is given in energy units, *i.e.* the Boltzmann factor k_B is omitted.

For actin filament networks, experimental and simulation studies have shown that the length of the filament has a rather small effect on the system properties. The mesh size of the network increases with the filament length, but otherwise the structure does not seem to vary strongly.[34,39–41] This is a very remarkable fact and, so far, there has been no detailed explanation for this length independence. Studying the dependence (or independence) of a crosslinked network on the system parameters is highly relevant, not only for a better insight into the physics of cells, but also for the development of new materials based on self-assembling networks. In this article, we study the percolation transition in a system of filaments and crosslinkers for various filament lengths. We use the model system with the spherocylindrical filaments and the short spherocylindrical crosslinkers, which has already been investigated systematically for a filament length of $l_F = 15D$, where D is the diameter of the spherocylinders.[42] The crosslinkers have a binding site at each end. Each site can bind to a filament that is mostly perpendicular to the crosslinker. Thus, the model mimics real crosslinkers in the cytoskeleton that are elongated and can bind to one filament at each end, while being preferentially perpendicular to the filament. Indeed, we observe that for a given volume fraction, the percolation threshold is rather independent of the length of the filaments. However, the percolation transition depends sensitively on the filament volume fraction.

We introduce an analytic approach that motivates why the filament volume fraction has a strong influence on the network formation, while the influence of the filament length at fixed volume fraction is low. This result and the corresponding analytic studies provide new important insights into the structural properties of the crosslinker-mediated formation of filament networks.

The article is structured as follows: in Section 2, we present details of the chosen model system. Results are shown in Section 3, while results and conclusions are summarized in Section 4. In the appendix, Section A, the effective adhesion volume is calculated, which is needed for the analytic considerations.

2 Model and simulation method

The filaments (f) and the crosslinking proteins (l) are approximated by spherocylinders of diameter D and length $L = l_F$ and $L = l_L$, respectively. A scheme of the model system and the notation of the relevant lengths and vectors are given in Fig. 1. Following a convention frequently used for spherocylinder systems, l_F and l_L denote the length of the cylinder axes so that
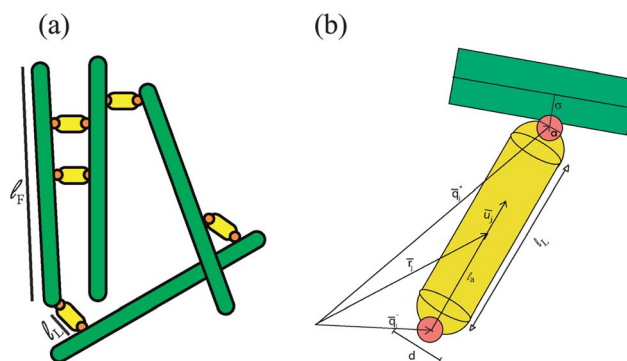
Fig. 1 (a) Scheme of a model system for the rods and linkers. The rods are approximated by hard spherocylinders and the crosslinkers by spherocylinders with a filament-adhering site on each end. Filaments and crosslinkers are taken to have the same diameter. (b) The schematic representation of a crosslinker. The crosslinker adheres to filaments through square well potentials which are located symmetrically on the cylindrical axis, at a distance of l_a from the center. The range of the square well diameter is denoted by a.

the maximum extensions are $l_F + D$ and $l_L + D$, respectively. Each spherocylinder j is determined by the position of its center of mass $\boldsymbol{r}_j$ and the unit vector $\boldsymbol{u}_j$ parallel to the cylindrical axis, which points from $\boldsymbol{r}_j - \frac{L}{2}\boldsymbol{u}_j$ to $\boldsymbol{r}_j + \frac{L}{2}\boldsymbol{u}_j$. A pair of rods belonging to the same class, that is, a pair of filaments or a pair of crosslinkers, interact through a purely repulsive hard-core potential

$$U_{hc}\left(\lambda_{ij}\right) \equiv \begin{cases} 0 & \text{if } \lambda_{ij} \geq D \\ \infty & \text{if } \lambda_{ij} < D \end{cases}, \tag{1}$$

where λ_{ij} is the shortest distance between the axes of a pair of spherocylinders, which is

$$\lambda_{ij} \equiv \min_{\substack{-1 \leq s_i \leq 1 \\ -1 \leq s_j \leq 1}} \left\| \left(\boldsymbol{r}_j + \frac{s_j L(j)}{2}\boldsymbol{u}_j\right) - \left(\boldsymbol{r}_i + \frac{s_i L(i)}{2}\boldsymbol{u}_i\right) \right\|. \tag{2}$$

In addition, the crosslinkers have an adhesive site at each end, which interacts with neighboring filaments *via* the attractive potential U_{ij}^{fl}. To define U_{ij}^{fl}, the quantities σ_{ij}^+ and σ_{ij}^- are introduced, which are the shortest distances between the adhesive sites of the crosslinker and the axis of the filament

$$\sigma_{ij}^{\pm} \equiv \min_{-1 \leq s_i \leq 1} \left\| \left(\boldsymbol{q}_j^{\pm}\right) - \left(\boldsymbol{r}_i + \frac{s_i l_F}{2}\boldsymbol{u}_i\right) \right\| \tag{3}$$

with $\boldsymbol{q}_j^{\pm} \equiv \boldsymbol{r}_j \pm l_a\boldsymbol{u}_j$. The adhesive segments, which are located symmetrically on both ends of the axis of the crosslinker, are a distance l_a away from the center of mass of the crosslinker. A crosslinker interacts with a filament through a single square-well attractive potential, which is defined as a function of the distance $\sigma_{ij}^{\pm}$ between the filament axis and the nearest adhesive site of the crosslinker, *via*

$$U_{sw}\left(\sigma_{ij}^{\pm}\right) \equiv \begin{cases} -\varepsilon & \text{if } \sigma_{ij}^{\pm} < a \\ 0 & \text{if } \sigma_{ij}^{\pm} \geq a \end{cases}. \tag{4}$$

The total interaction potential between a filament and a crosslinker is given by

$$U_{ij}^{fl} = U_{hc}(\lambda_{ij}) + U_{sw}(\sigma_{ij}^{\pm}). \tag{5}$$

In our model, the preferred alignment of a crosslinker rod adhering to a filament rod is determined by the location, $q^{\pm}$, of the adhesive site and the range of the square-well potential a. If a is set to be reasonably small and the position of the adhesive site is located at a point within the spherical cap of the spherocylinder, the alignment of the adhering crosslinker rod to the filament rod is limited to angles close to $\pi/2$. Furthermore, with such a construction it can be assured that one adhesive site of a crosslinker does not simultaneously interact with more than one filament.

In our simulations, we studied rod lengths $l_F/D = 10, 15, 20$, and 25, while the length of crosslinkers is $l_L = 2D$. The square-well diameter a, which defines the range of the filament-adhering potential of the crosslinker, is set to $a = 0.7D$. The square well potentials were placed symmetrically along the cylindrical axes, at a distance of $l_a = 1.35D$ from the center of mass of the crosslinkers.

Filaments and crosslinkers have volumes $V_f = \pi \frac{D^2}{4}\left(l_F + \frac{2}{3}D\right)$ and $V_l = \pi \frac{D^2}{4}\left(l_L + \frac{2}{3}D\right)$, respectively. For a system of N_f filaments and $N_l = n_{lf} N_f$ crosslinkers of length $l_L = 2D$, the ratio of the crosslinker volume fraction Φ_l and the filament volume fraction Φ is given by $\frac{\Phi_l}{\Phi} = \frac{8}{3} n_{lf} \left(\frac{l_F}{D} + \frac{2}{3}\right)^{-1}$. If we keep Φ_l/Φ fixed, the crosslinker–filament ratio n_{lf} is approximately proportional to the filament length $n_{lf} \simeq \frac{3}{8}\frac{\Phi_l}{\Phi}\frac{l_F}{D}$ for $l_F \geq 10D$.

In order to create an initial configuration, the filaments and crosslinkers were first arranged on a simple tetragonal lattice. The values of N_f, N_l and the volume V were chosen in order to generate initial configurations for values of Φ varying between 0.02 and 0.05 while keeping $n_{lf} = 2.0$. If not mentioned differently, we use $N_f = 500$. The length of the filaments sets a lower limit to the simulation box size, whose side length $V^{1/3}$ is always set to be greater than $2l_F$. The cubic lattice arrangements were equilibrated to an isotropic fluid of filaments and crosslinkers, in the absence of attractive interactions, i.e. $\varepsilon = 0$, using a constant volume (NVT) Monte Carlo simulation. The equilibrium configurations were reached by translational and rotational moves of the filaments and crosslinkers. For a system of N_f filaments and N_l crosslinkers, $2(N_f + N_l)$ attempts of an orientational or translational move are made for every sweep.

After 2×10^5 sweeps, the adhesive square-well potential is switched on and for various values of Φ, simulations are performed with a set of different adhesion strengths ε. All simulations were started individually with the described method. In most cases, we chose a fixed filament–crosslinker ratio $n_{lf} = 2.0$ as Φ and ε were varied, but we also studied the system behavior while keeping Φ_l/Φ fixed.

Additionally, simulations were performed with different system sizes in order to examine finite size effects. The number of sweeps required to equilibrate ranges from 5×10^6 to 2×10^7, depending on the filament volume fraction and the crosslinker concentration. The systems were equilibrated before averages were taken.

3 Simulation results

Using Monte Carlo simulations, the system is analyzed for various parameter values. In the absence of the adhesive square-well potential, i.e. for $\varepsilon = 0$, the filaments and crosslinkers form an isotropic fluid. With adhesive potentials, the average number of crosslinkers adhering to the filaments increases with ε. Each crosslinker can bind up to two filaments, one at each adhesive site. In the following, a pair of filaments is called connected if they bind to the same crosslinker.

A filament can be connected to several other filaments through an attractive interaction mediated by one or more crosslinkers. A group of filaments form a cluster if each pair of filaments is associated by a chain of connected filaments. The size of a cluster is taken to be the number of filaments in the cluster.

3.1 Percolation

The connectivity of the filament system is analyzed with the help of percolation theory,[57–59] where the formation of a long range network is treated as a percolation transition. In an infinite system, a percolation transition is marked by the formation of an infinitely large cluster which spans the entire system. For finite system sizes, the fraction of monomers in the largest cluster $\langle s_{max}\rangle$ can be taken as an order parameter.[60,61] A value of $\langle s_{max}\rangle = 1$ corresponds to a system in which all filaments are connected to the same cluster.

$\langle s_{max}\rangle$ is plotted as a function of adhesion strengths ε, for various rod lengths between $l_F = 10D$ and $l_F = 25D$ in Fig. 2. At low ε the rods do not form a cluster and $\langle s_{max}\rangle$ is zero. As ε is increased, small clusters form and grow; hence $\langle s_{max}\rangle$ increases. For $\langle s_{max}\rangle = 0.5$, the largest cluster contains half of the total number of rods in the system. Simulation studies of the percolation transition have shown that the percolation threshold $\tilde{\varepsilon}$ of the infinite system is well approximated by the value of ε for which $\langle s_{max}\rangle = 0.5$.

The data shown in Fig. 2 provide the main result of this article. Remarkably, for $n_{lf} = 2$ and fixed Φ, the dependence of the transition threshold on the filament length is very small. For rod
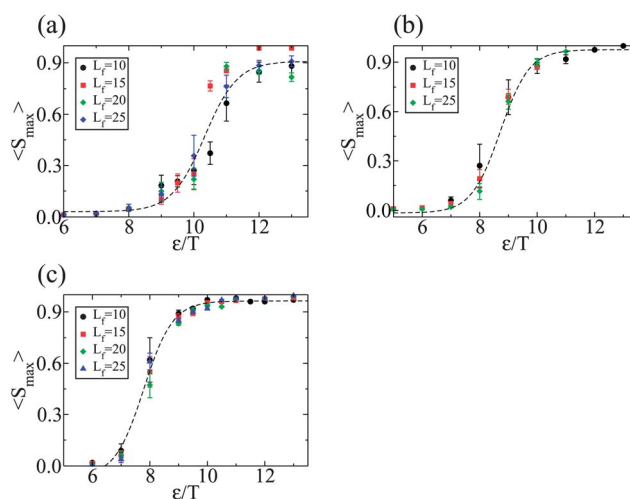
Fig. 2 The average fraction of rods $\langle s_{max}\rangle$ that are part of the largest cluster as a function of adhesion strength ε for filament volume fraction $\Phi \simeq$ (a) 0.02, (b) 0.03, and (c) 0.05. Different symbols correspond to different rod lengths: $l_F = 10D(\bullet)$, $l_F = 15D(\blacksquare)$, $l_F = 20D(\blacklozenge)$, and $l_F = 25D(\blacktriangle)$.
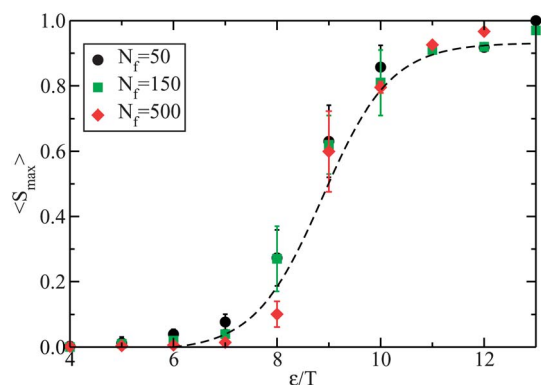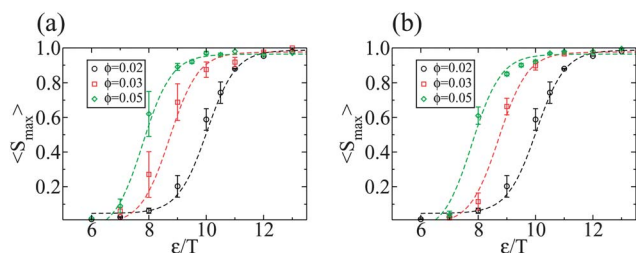
Fig. 3 The average fraction of rods $\langle s_{\max} \rangle$ that are part of the largest cluster as a function of adhesion strength ε for various system sizes, for filament length $l_F = 10D$, filament volume fraction $\Phi_f = 0.03$ and crosslinker–filament ratio $n_{lf} \simeq 2$.

Fig. 5 The average fraction of rods $\langle s_{\max} \rangle$ that are part of the largest cluster as a function of adhesion strength ε for various rod lengths. The ratio of volume fractions of filaments and crosslinkers, $\Phi_l/\Phi \simeq 2.0$, for all rod lengths. Since the filament volume fraction $\Phi \simeq 0.03$, the crosslinker–filament ratio n_{lf} is larger for longer rods.
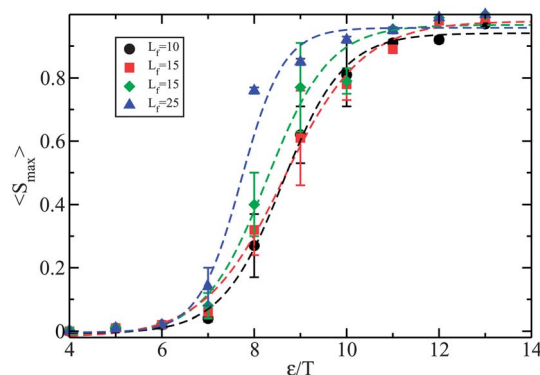
lengths between $l_F = 10D$ and $l_F = 25D$ the data points of $\langle s_{\max} \rangle$ can approximately be fitted by the same curve. This is especially true for larger filament volume fractions $\Phi = 0.03$ (b) and $\Phi = 0.05$ (c) while deviations are stronger for $\Phi = 0.02$. We have studied the influence of finite size effects (see Fig. 3) by varying the system size with fixed $l_F = 10D$, $\Phi = 0.03$, and $n_{lf} = 2$. Below the percolation threshold the values of $\langle s_{\max} \rangle$ are a bit smaller for larger system sizes, *i.e.* larger N_f. However, the effects are too small to extract a scaling law from the accessible range of system sizes.

While in the studied range $\tilde{\varepsilon}$ depends only weakly on the filament length (see Fig. 2), it decreases significantly with increasing filament volume fraction Φ. This is shown clearly in Fig. 4, where $\langle s_{\max} \rangle$ vs. ε has been plotted for various Φ. Results are shown for $l_F = 10D$ and $l_F = 25D$ in Fig. 4(a) and (b), respectively.

It is interesting to study the influence of the filament length if the ratio of crosslinker and filament volume fractions Φ_l/Φ is kept fixed, rather than n_{lf}. In this case, the ratio of n_{lf}/l_F is approximately fixed, which means that the ratio of actin and crosslinker monomers is fixed as the filament length is varied. Fig. 5 shows $\langle s_{\max} \rangle$ as a function of ε/T for different filament lengths with fixed $\Phi_l/\Phi = 2.0$. If Φ_l/Φ is kept fixed, percolation is clearly supported by larger filament lengths. In contrast, the percolation behavior is independent of the filament length if the number of crosslinkers per filament n_{lf} is fixed. For a simplified model system this will be analyzed in Section 3.3.

3.2 Cluster size distribution and cluster structure

Right at the percolation threshold, the cluster size distribution n_s of an infinite system shows a power-law decay[58,59] $n_s \propto s^{-\tau}$, with the Fisher exponent τ, which corresponds to the negative slope of the straight line found in a log–log plot. For a finite system size, the power law behavior is restricted to small cluster sizes, while for lengths s of the order of the system size it naturally breaks down. Fig. 6 shows n_s at $\Phi \simeq 0.05$ for various rod lengths at $\tilde{\varepsilon} = 8T$ close to the percolation threshold. The hump in the cluster size distribution caused by the finite system size is excluded from the power-law fit, which then gives a Fisher exponent, $\tau \simeq 2.5$, for all values of l_F.

It is instructive to compare our system with networks of flexible, randomly crosslinked polymers. If the polymers consist of short multifunctional monomers, the system has a Fisher exponent of $\tau \simeq 2.2$.[62] However, long linear polymers that are interconnected by short agents, as found in polymer systems after a vulcanization process,[63] are described well by the Flory–Stockmayer theory.[64–66] This theory holds up well in very close distance to the percolation threshold and predicts a Fisher exponent of $\tau \simeq 2.5$.[67] For all studied rod lengths, from $l_F = 10D$ to $l_F = 25D$, the Fisher exponent is $\tau \simeq 2.5$, just as for the
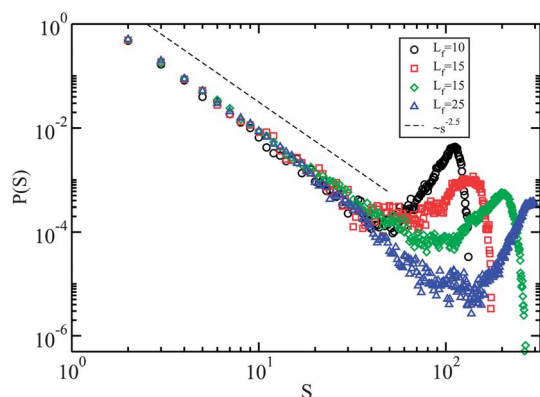

Fig. 4 The average fraction of rods $\langle s_{\max} \rangle$ that are part of the largest cluster as a function of adhesion strength ε, for rod lengths (a) $l_F = 10D$ and (b) $l_F = 25D$. Results are shown for $\Phi \sim 0.02 (\bigcirc)$, $\Phi \sim 0.03 (\square)$, and $\Phi \sim 0.05 (\diamondsuit)$.

Fig. 6 Cluster size distribution close to percolation transition for various filament lengths, at filament volume fraction $\Phi \sim 0.05$ and $\varepsilon = 8T$.

vulcanization class of crosslinked polymers. This is remarkable, since the theory by de Gennes that predicts this behavior assumes that the polymer follows a random path between the crosslinkers. According to our results, this is not necessary and the length of the straight connection between the links seems to have no impact within the studied range of rod lengths.
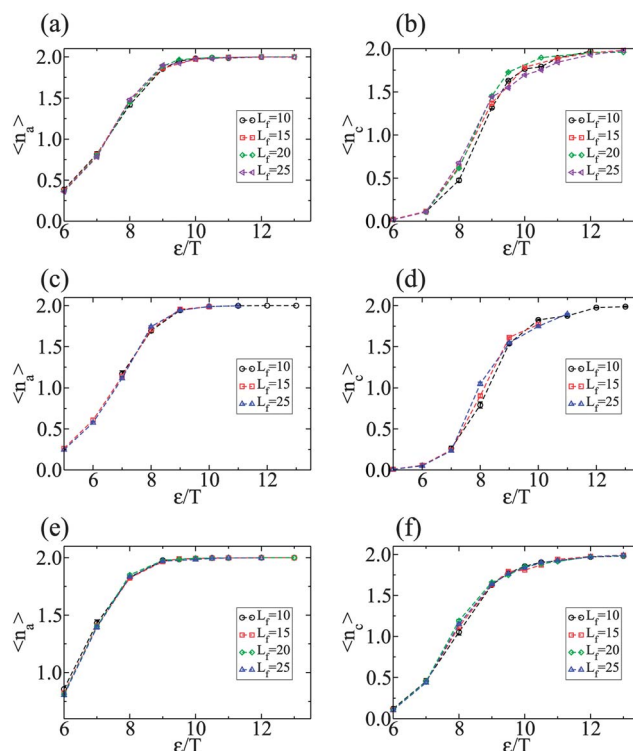
3.3 Average number of adhering linkers and connectors

The simulation results show that, for a given filament volume fraction Φ, the percolation threshold depends only weakly on the filament length. This is not a matter of course. While the Fisher exponent is universal in its material class, the transition threshold is not. It is of interest to study the average number of *adhering linkers*, *i.e.* crosslinkers that adhere to at least one filament, and the average number of *connectors*, crosslinkers that adhere to two filaments. According to network theory, we can consider the filaments as "nodes" forming a network with the help of the connectors that serve as links. Now the connectivity of the network depends on the average connectors per node, corresponding to the number of connecting crosslinkers per filament. Fig. 7(a), (c) and (e) show the average number of adhering crosslinkers per filament $\langle n_a \rangle$ for $\Phi = 0.02$, $\Phi = 0.03$, and $\Phi = 0.05$. For large adhesion strengths ε the curves converge to a value of $\langle n_a \rangle = 2$, corresponding to the chosen crosslinker–filament ratio of $n_{lf} = 2$. In Fig. 7(b), (d) and (f), the average number of connectors $\langle n_c \rangle$ is shown. Also these curves converge to a value of 2 with increasing ε, but, as expected, they converge more slowly. The curves of $\langle n_a \rangle$ show a negligible dependence on l_F. For $\langle n_c \rangle$, a weak dependence on l_F is visible, where a slightly higher connectivity is found for longer rods.

In order to study the adhesion behavior of crosslinkers in more detail, we introduce a simple analytical model. First, we consider one filament and a crosslinker in its vicinity. Whether the crosslinker binds or not depends on the location and the orientation of the crosslinker. Let ϑ be the angle between the axis of the crosslinker and the surface normal of the filament and φ the corresponding azimuthal angle. For given angles ϑ and φ, the center of mass of an adhering crosslinker must lie within a certain volume around the filament, which we call the *adhesion volume* $v_{ad}(\vartheta,\varphi)$ of the filament (see Fig. 8(a)). If the crosslinker is strongly tilted to the filament surface normal, the adhesion volume vanishes. Otherwise, its shape is similar to a spherocylindrical shell around the filament. For $\vartheta = 0$, the adhesion volume is bounded by two spherocylinders with axis length l_F, where the inner one has a radius $\frac{l_L}{2} + D$ and the outer one has a radius $a + l_a$. We define the effective adhesion volume per filament v_{ad}^* as the adhesion volume $v_{ad}(\vartheta,\varphi)$, averaged over all angles. An expression for v_{ad}^* is derived in the appendix. With the values $l_L = 2D$, $l_a = 1.35D$, and $a = 0.7D$, used in the simulations, one has

$$v_{ad}^* \simeq k_1 D^2 l_F \left(1 + k_2 \frac{D}{l_F}\right) \qquad (6)$$

with $k_1 \equiv 0.0136$ and $k_2 \equiv 2.36$. Now we consider a dilute system of N_f filaments and N_l crosslinkers. With the total effective adhesion volume $V_{ad}^* \simeq N_f v_{ad}^*$, the probability that a given crosslinker is adhering is approximately given by

Fig. 7 Average number of adhering crosslinkers per filament n_a/N_f (a, c and e), and average number of connectors per filament n_c/N_f (b, d and e), for various filament volume fractions Φ. $\Phi \simeq 0.02$ (a and b), $\Phi \simeq 0.03$ (c and d), $\Phi \simeq 0.05$ (e and f). Different symbols correspond to different rod lengths. $l_F = 10D$ ($\bigcirc$), $l_F = 15D$ ($\square$), $l_F = 20D$ ($\triangle$), and $l_F = 25D$ ($\diamond$).

$$P_{ad} \simeq \frac{V_{ad}^* e^{\beta\varepsilon}}{\left(V_{acc} - V_{ad}^*\right) + V_{ad}^* e^{\beta\varepsilon}} \simeq \frac{V_{ad}^* e^{\beta\varepsilon}}{V_{acc} + V_{ad}^* e^{\beta\varepsilon}} \qquad (7)$$

where V_{acc} is the part of the total volume V that can be accessed by the center of mass of the crosslinker.
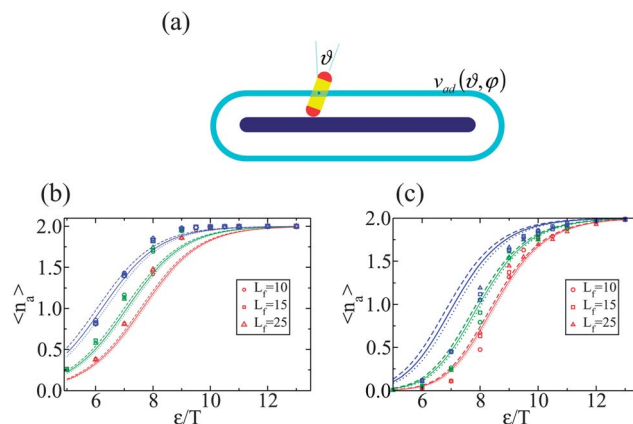
Fig. 8 (a) The analytic approach is based on the adhesion volume $v_{ad}(\vartheta,\varphi)$. The adhesion volume is a shell around the filament and depends on the angles ϑ and φ with respect to the local surface normal and the symmetry axis of the filament. (b) Average number of adhering crosslinkers per filament n_a. (c) Average number of connecting crosslinkers per filament n_c; analytical model (curves) compared with simulation data (symbols). Plots are shown for filament volume fractions $\Phi = 0.05$ (blue), $\Phi = 0.03$ (green), $\Phi = 0.03$ (red), each with $l_F = 10D$ (---)($\bigcirc$), $l_F = 15D$ (—)($\square$), $l_F = 25D$ ($\cdots$)($\triangle$).

For a dilute system of hard spherocylinders, the accessible volume, averaged over all orientations, is approximately

$$V_{\text{acc}} \simeq V - N_{\text{f}} v_{\text{lf}}^x - \tfrac{1}{2} N_{\text{l}} v_{\text{ll}}^x \qquad (8)$$

where v_{lf}^x is the average excluded volume between a crosslinker and filament, while v_{ll}^x is the average excluded volume between two crosslinkers. The factor 1/2 corrects the double counting of crosslinkers. Averaged over all orientations, the excluded volume of two spherocylinders of lengths L_1 and L_2 and diameter D is given by[68,69]

$$v_{12}^x = \frac{\pi D}{6}\big(3(L_1 + 2D)(L_2 + 2D) - 4D^2\big). \qquad (9)$$

We obtain an expression for the average number $\langle n_{\text{a}} \rangle$ of adhering crosslinkers per filament in a dilute system:

$$\langle n_{\text{a}} \rangle_{\text{theo}} \simeq n_{\text{lf}} P_{\text{ad}} = n_{\text{lf}} \left(1 + \frac{V_{\text{acc}}}{V_{\text{ad}}^*} e^{-\beta \varepsilon}\right)^{-1}. \qquad (10)$$

The number of filaments is given by

$$N_{\text{f}} = \Phi V_{\text{f}} V^{-1} = \Phi V^{-1} \pi \frac{D^2}{4}\left(l_{\text{F}} + \frac{2}{3}D\right) \qquad (11)$$

with the filament volume V_{f}. Thus, one has

$$\frac{V_{\text{acc}}}{V_{\text{ad}}^*} = \frac{\Phi^{-1} V_{\text{f}} - \left(v_{\text{lf}}^x - \dfrac{n_{\text{lf}}}{2} v_{\text{ll}}^x\right)}{v_{\text{ad}}^*} \qquad (12)$$

For a sufficiently diluted system with l_{a}, l_{L}, and a as used in our simulations one has

$$\lim_{l_{\text{F}} \to \infty}\left(\frac{V_{\text{acc}}}{V_{\text{ad}}^*}\right) \simeq \frac{231}{4}\left(\Phi^{-1} - 8\right) \qquad (13)$$

in the limit of large filament lengths l_{F}. However, also for finite filament lengths like those chosen in the simulations, the impact of l_{F} on the average number of attached crosslinkers per filament is comparably low. So far we have assumed that n_{lf} is a constant, independent of l_{F}. If we keep the ratio Φ_{l}/Φ of crosslinker and filament volume fractions fixed, then n_{lf} increases approximately linearly with l_{F}. As a consequence, percolation sets in earlier as shown in Fig. 5.

In Fig. 8(b), $\langle n_{\text{a}} \rangle_{\text{theo}}(\varepsilon)$ is shown for various filament lengths and filament volume fractions. It turns out that, especially for low ε, the curves are in fair agreement with the simulation results. This is remarkable, since eqn (10) does not depend on any fit parameter. Like the simulation data, $\langle n_{\text{a}} \rangle(\varepsilon)$ depends much less on the filament length than on the filament volume fraction. At higher ε, the simulation values of $\langle n_{\text{a}} \rangle(\varepsilon)$ increase faster than $\langle n_{\text{a}} \rangle_{\text{theo}}(\varepsilon)$. This indicates that correlations between the rods become relevant that are neglected in the low density approach. Apparently, the filaments arrange in such a way that adhesion of crosslinkers is promoted. However, on the whole range of ε, the simple analytical approach describes the attachment probability rather well, which indicates that correlations and many-particle interactions have a minor influence on this quantity.

A rough estimate for the average number of connectors per filament $\langle n_{\text{c}} \rangle_{\text{theo}}(\varepsilon)$ is given by

$$\langle n_{\text{c}} \rangle_{\text{theo}} \simeq n_{\text{lf}}(P_{\text{ad}})^2. \qquad (14)$$

This equation reflects that a connector has to adhere to two filaments, assuming that each event occurs with the probability found in eqn (7). One would expect that binding to a second filament is less probable for an attached crosslinker. Thus, eqn (14) should overestimate the average number of connectors. As shown in Fig. 8(c), this is indeed the case for $\Phi = 0.05$, the highest filament volume fraction considered. For lower filament volume fractions $\Phi = 0.02$ and $\Phi = 0.03$, the values of $\langle n_{\text{c}} \rangle_{\text{theo}}$ fit surprisingly well to the simulated data. At lower ε, eqn (14) slightly overestimates the number of connectors, while at higher ε, the simulated values increase more strongly, which again may reflect the fact that the system adapts to the presence of many connecting crosslinkers and facilitates the formation of new connections. In the theoretical as well as in the simulation data, the influence of the filament length on N_{C} is low. Thus, the linking probability between the filaments does not depend strongly on l_{F} at fixed filament volume fraction.

In terms of network theory we can view our model system as a set of nodes interconnected by (crosslinker) bonds, where the average number of bonds $\langle n_{\text{c}} \rangle$ per node depends only weakly on l_{F}. This does not imply that $\tilde{\varepsilon}$ is independent of l_{F}. In general, $\tilde{\varepsilon}$ may depend on several other system properties. The bond percolation thresholds have been calculated for various regular three-dimensional lattices like the simple cubic, the face centered cubic and the body centered cubic lattices,[70] the hexagonal close-packed lattice[71] or the diamond lattice.[72] It turns out that the probability of bond formation P_{thresh} at the percolation threshold depends strongly on the given crystal lattice. However, the average number of bonds per node $\langle n_{\text{c}} \rangle_{\text{thresh}} = P_{\text{thresh}} m/2$ with coordination number m lies in the range of 0.72 to 0.78 for the mentioned lattices. We note that the threshold values for $\langle n_{\text{c}} \rangle_{\text{thresh}}$ are all higher than those found for the regular lattices. Furthermore, they depend strongly on the packing fraction. For $\Phi = 0.02$, $\Phi = 0.03$, and $\Phi = 0.05$ one has $\langle n_{\text{c}} \rangle_{\text{thresh}} = 1.8 \pm 0.1$, $\langle n_{\text{c}} \rangle_{\text{thresh}} = 1.4 \pm 0.2$, and $\langle n_{\text{c}} \rangle_{\text{thresh}} = 1.1 \pm 0.2$. This phenomenon can be explained rather easily. As reported in ref. 42 the system tends to form bundles of parallel rods, which are interconnected by various crosslinkers. However, for each pair of rods there is only one connector that contributes to the connectivity of the network, and every additional connector is redundant. Thus, the more the bundles are formed in the system the higher is the threshold value of $\langle n_{\text{c}} \rangle$. As shown in ref. 42 the amount of rods involved in bundles decreases with increasing filament volume fraction. At low volume density, the formation of parallel rods in a bundle enables a larger number of connectors. Every time, two filaments are connected by more than one crosslinker, and the additional connectors are not available to support the interconnectivity of the system. Therefore, in systems with pronounced bundling, more connectors are required for percolation. Apparently, the percolation threshold depends on the average number of connectors per filament and on the typical alignment of neighboring filaments. Since neither $\langle n_{\text{c}} \rangle(\varepsilon)$ nor $\tilde{\varepsilon}$ depends strongly on l_{F} we expect that also the orientation of connected filaments should not depend strongly on the filament length.

We have measured the probability distribution of mutual alignment between a pair of connected filaments, averaged over all pairs of filaments. In Fig. 9 the probability distribution P is plotted against $\cos \theta$ for $\Phi = 0.05$ and $\varepsilon = 10T$, where $\theta \leq \pi/2$ is the acute angle between two connected filaments. One can see
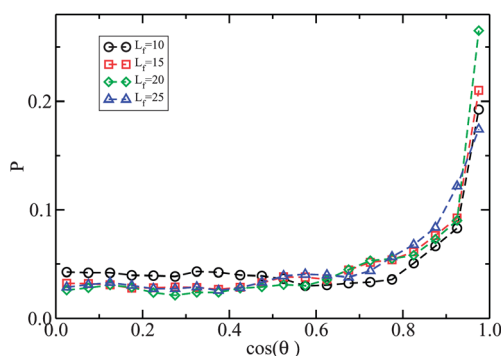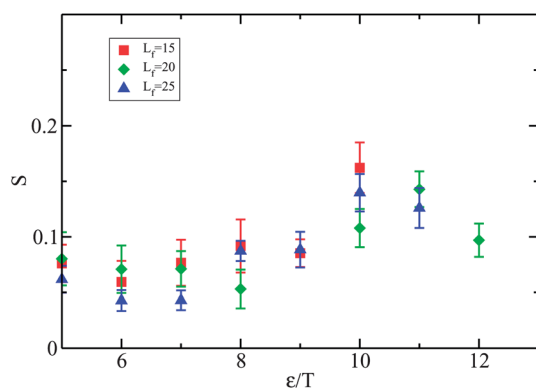
Fig. 9 Distribution of $\cos(\theta)$, with $\theta \leq \pi/2$ being the acute angle made by a pair of connected filaments. Results are shown for filaments of various lengths l_F, at $\varepsilon \simeq 10T$ and $\Phi \simeq 0.05$. The peak at $\cos\theta \sim 1$ indicates that a majority of adhering filaments are parallel to each other.

that this distribution is not strongly dependent on the filament length, as assumed. In Fig. 10, the nematic order parameter S is shown for different filament lengths as a function of the adhesion strength. For systems with $n_{lf} = 2$, the orientational order is low for $\varepsilon/T \leq 9$. At the percolation threshold $\varepsilon/T \simeq 10$, the order parameter reaches slightly larger values up to $S \simeq 0.15$. Thus, while connected rods are strongly aligned (see Fig. 9), the overall orientational order in the system is low. Furthermore, the data in Fig. 10 show no significant dependence on the rod length.

4 Conclusions

Using Monte Carlo simulations and an analytic approach we have studied a model system of a self-assembling filament network. The network consists of spherocylindrical rods and spherocylindrical crosslinkers that can bind on both ends to the filaments. We have investigated the length dependence of the percolation threshold $\tilde{\varepsilon}$ as a function of the filament length l_F and filament volume fraction Φ. If we keep the ratio of volume fractions Φ_l/Φ constant, percolation is promoted by bigger rod lengths.

A very remarkable result is found if the rod length is changed while the crosslinker–filament ratio n_{lf} and the filament volume fraction Φ are kept fixed: In this case, the percolation threshold is rather independent of l_F. A Fisher exponent of $\tau \simeq 2.5$ was

determined for all rod lengths. The same value has been calculated for the class of vulcanized polymers. We found that also the average number of adhering crosslinkers and the average number of connectors do not depend strongly on the filament length. These trends could be reproduced by a simple analytical model. At low ε, it reproduces the values found in the simulation surprisingly well, even though correlations in the system are mostly neglected by the theoretical approach. Finally, we find that the angular distribution of filaments is not strongly dependent on l_F in the simulation. Altogether, many quantities, like $\langle n_a \rangle$, $\langle n_c \rangle$, the angular distribution between connecting filaments, and finally $\tilde{\varepsilon}$ vary strongly with the filament volume fraction but are rather robust against changes of l_F. This robustness is of great help for the study of self-assembling filament networks, since it reduces the number of relevant parameters. It simplifies the interpretation of experimental structure data of F-actin filament networks and similar cross-linked polymer systems.

It is interesting to compare our results with those of Nguyen *et al.*[39,40] They have studied actin networks experimentally and with coarse-grained molecular dynamics simulations. Increasing the crosslinker–filament ratio leads to a more pronounced bundling, in accordance with our previous simulations.[42] The experimental and the computational studies show that the lengths of the filaments have a minor influence on the system properties, which corresponds to the results in this paper. However, they also found that within the studied range the filament concentration does not strongly change the structure of the network. This result differs from our findings. We assume that the different observations are related to the fact that the filament packing fraction in our systems is generally larger. While in the simulations of Nguyen *et al.* the packing fraction is always below 0.001, we have studied packing fractions Φ in the range between 0.003 and 0.05 (see also ref. 42). Obviously the influence of the packing fraction is especially low in dilute systems. From eqn (12) and (14) it follows that for low Φ the number of connectors $\langle n_c \rangle_{theo}$ is proportional to Φ^2 so that the dependence of $\langle n_c \rangle_{theo}$ on Φ increases with the filament packing fraction Φ.

With our theoretical approach we could show that the number of adhering linkers is not strongly dependent on l_F, because the effective adhesion volume depends rather on Φ than on l_F. Other aspects that lead to the robustness of the percolation threshold against changes of the filament length and the surprisingly good matching between simulation data of $\langle n_c \rangle(\varepsilon)$ and the results found with the simple theoretical approach that neglects all higher order correlations are not yet understood and remain to be investigated in the future. There are other aspects that would be of great interest for future studies. It is important to investigate the influence of the crosslinker length on the network structure. Another point that should be addressed is the finite rigidity of the filaments, which may be studied with semiflexible polymers rather than with hard spherocylinders. The good agreement between the Fisher exponent found for our model system and that predicted for crosslinked polymer networks indicates that many aspects of systems with semiflexible filaments are already represented in our model with rigid rods, but the influence of the elasticity of filaments should be analyzed in detail.

Fig. 10 The nematic order parameter S as a function of the adhesive strength ε for $n_{lf} = 2$ and various rod lengths.

A Appendix

A.1 Calculating the effective adhesion volume

We consider orthonormal basis vectors e_x, e_y, e_z and a filament at the origin, oriented parallel to e_x. One crosslinker has the center of mass at the point me_z and its symmetry axis parallel to

$$\boldsymbol{u}_1 = \cos(\varphi)\sin(\vartheta)\boldsymbol{e}_x + \sin(\varphi)\sin(\vartheta)\boldsymbol{e}_y + \cos(\vartheta)\boldsymbol{e}_z, \quad (15)$$

as shown in Fig. 11. The lower adhesive site $\boldsymbol{q}$ is localized at

$$\boldsymbol{q} = m\boldsymbol{e}_z - l_a\boldsymbol{u}_1 \quad (16)$$

and the end of the cylinder axis $\boldsymbol{c}$ on that side is given by

$$\boldsymbol{c} = m\boldsymbol{e}_z - \frac{l_L}{2}\boldsymbol{u}_1. \quad (17)$$

For an adhering crosslinker the distance between $\boldsymbol{q}$ and the filament axis must be smaller than a. One obtains the condition
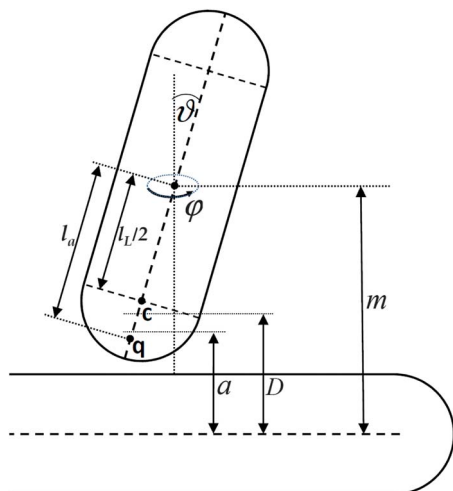
$$m \leq m_{\text{max}} \equiv l_a\cos(\vartheta) + \sqrt{a^2 + l_a^2\sin^2(\varphi)(1 - \cos^2(\vartheta))}. \quad (18)$$

Since $\cos(\vartheta)$ is close to one, m_{max} can be linearized with respect to $(\cos(\vartheta) - 1)$. Then, averaging over all φ leads to

$$m_{\text{max}} \simeq a - \frac{l_a^2}{2a} + l_a\left(1 + \frac{l_a}{2a}\right)\cos(\vartheta). \quad (19)$$

Analogously, we can determine a lower limit m_{min} for m by considering that, due to steric interactions, the distance between $\boldsymbol{c}$ and the filament axis has to be larger than D:

$$m_{\text{min}} \simeq D - \frac{l_L^2}{8D} + \frac{l_L}{2}\left(1 + \frac{l_L}{4D}\right)\cos(\vartheta). \quad (20)$$

Fig. 11 The angles ϑ and φ are the polar angles of the crosslinker axis in a basis, determined by the normal of the adjacent filament surface and the filament axis. Then, the crosslinker binds if its center lies within the adhesion volume $v_{\text{ad}}(\vartheta,\varphi)$. The width of the adhesion volume is determined by the fact that the adhesion site $\boldsymbol{q}$ must be smaller than a, while the distance of the end of the cylinder axis of the crosslinker $\boldsymbol{c}$ must be larger than D.

Since m_{min} must not be larger than m_{max} the angle ϑ has to be smaller than

$$\vartheta_{\text{max}} = \arccos\left(\frac{8aD(D - a) + 4Dl_a^2 - al_L^2}{4Dl_a(2a + l_a) - al_L(4D + l_L)}\right) \quad (21)$$

We now define an *adhesion volume* v_{cyl} around the cylindrical part of the filament. A crosslinker with a given angle $\vartheta \leq \vartheta_{\text{max}}$ binds if its center of mass lies within a cylindrical shell of width $w(\vartheta) = m_{\text{max}}(\vartheta) - m_{\text{min}}(\vartheta)$ and length l_F. In good approximation the volume of the cylindrical shell is given by

$$v_{\text{cyl}} = wA \quad (22)$$

with $A = 2\pi\left(D + \frac{l_L}{2}\right)l_F$. Now we average v_{cyl} over all angles ϑ and obtain the cylindrical part of the effective adhesion volume per filament

$$v_{\text{cyl}}^* = w^*A \quad (23)$$

with

$$w^* = \frac{2\int_0^{\vartheta_{\text{max}}}(m_{\text{max}} - m_{\text{min}})\sin(\vartheta)\,\mathrm{d}\vartheta}{\int_0^{\pi}\sin(\vartheta)\,\mathrm{d}\vartheta}, \quad (24)$$

where the factor of 2 considers the two adhesive sites of the crosslinker. Insertion into eqn (23) leads to

$$v_{\text{cyl}}^* = l_F\frac{C_1}{C_2} \quad (25)$$

with

$$C_1 \equiv 2\pi aD\left(D + \frac{l_L}{2}\right)\left(a + l_a - D - \frac{l_L}{2}\right)^2, \quad (26)$$

$$C_2 \equiv aD(D - a) + D(a + l_a)^2 - a\left(D + \frac{l_L}{2}\right)^2. \quad (27)$$

The adhesion volume v_{caps}^* at the spherical caps of the filament can be calculated analogously. With the constants C_1 and C_2 from eqn (26) and (27), one finds

$$v_{\text{caps}}^* = \frac{C_1\left(D + \frac{l_L}{2}\right)}{C_2 - aD\left(l_a - \frac{l_L}{2}\right)}. \quad (28)$$

For the values chosen in the simulations, the effective adhesion volume

$$v_{\text{ad}}^* \equiv v_{\text{cyl}}^* + v_{\text{cap}}^* \quad (29)$$

of one filament is approximately

$$v_{\text{ad}}^* \simeq k_1D^2l_F\left(1 + k_2\frac{D}{l_F}\right) \quad (30)$$

with $k_1 \equiv 0.0136$ and $k_2 \equiv 2.36$.

References

1 J. S. Seo, D. Whang, H. Lee, S. I. Jun, J. Oh, Y. J. Jeon and K. Kim, *Nature*, 2000, **404**, 982.
2 M. E. Davis, *Nature*, 2002, **417**, 813.
3 S. Kitagawa, R. Kitaura and S. Noro, *Angew. Chem., Int. Ed.*, 2004, **43**, 2334.
4 A. Star, V. Joshi, S. Skarupo, D. Thomas and J. P. Gabriel, *J. Phys. Chem. B*, 2006, **110**, 21014.
5 E. L. Gui, L.-J. Li, K. Zhang, Y. Xu, X. Dong, X. Ho, P. S. Lee, J. Kasim, Z. X. Shen, J. A. Rogers and S. G. Mhaisalkar, *J. Am. Chem. Soc.*, 2007, **129**, 14427.
6 E. S. Snow, F. K. Perkins, E. J. Houser, S. C. Badescu and T. L. Reinecke, *Science*, 2005, **307**, 1942.
7 P. Hu, J. Zhang, Z. Wen and C. Zhang, *Nanotechnology*, 2011, **22**, 1.
8 S. Kumar, J. Y. Murthy and M. A. Alam, *Phys. Rev. Lett.*, 2005, **95**, 066802.
9 R. A. Villamizar, A. Maroto and F. X. Rius, *Sens. Actuators, B*, 2009, **136**, 451.
10 A. Vijayaraghavan, M. Y. Timmermans, K. Grigoras, A. G. Nasibulin, E. I. Kauppinen and R. Krupke, *Nanotechnology*, 2011, **22**, 265715.
11 A. V. Kyrylyuk, M. C. Hermant, T. Schilling, B. Klumperman, C. E. Koning and P. van der Schoot, *Nat. Nanotechnol.*, 2011, **6**, 364.
12 M. Hazani, D. Shvarts, D. Peled, V. Sidorov and R. Naaman, *Faraday Discuss.*, 2006, **131**, 325.
13 K. Keren, R. S. Berman, E. Buchstab, U. Sivan and E. Braun, *Science*, 2003, **302**, 1380.
14 G. Gruner, *Anal. Bioanal. Chem.*, 2006, **384**, 322.
15 R. Chelakkot, R. Lipowsky and T. Gruhn, *Macromolecules*, 2006, **39**, 7138.
16 J. Preuschen, S. Menchen, N. A. Winnik, A. Heuer and H. W. Spiess, *Macromolecules*, 1999, **32**, 2690.
17 P. G. Khalatur, A. R. Khokhlov, J. N. Kovalenko and D. A. Mologin, *J. Chem. Phys.*, 1999, **110**, 6039.
18 H. Lodish, P. Matsudaira, A. Berk, S. L. Zipursky, J. Darnell, H. F. Lodish, C. A. Kaiser, M. Krieger, M. P. Scott and M. Sahimi, *Molecular Cell Biology*, W.H. Freeman and Co, San Francisco, 5th edn, 2003.
19 E. L. F. Holzbaur and Y. E. Goldman, *Curr. Opin. Cell Biol.*, 2010, **22**, 4.
20 R. D. Vale, *Cell*, 2003, **112**, 467.
21 M. A. Titus and S. P. Gilbert, *Cell. Mol. Life Sci.*, 1999, **56**, 181.
22 R. Lipowsky, Y. Chai, S. Klumpp, S. Liepelt and M. J. I. Müller, *Physica A*, 2006, **372**, 34.
23 T. D. Pollard and J. A. Cooper, *Science*, 2009, **326**, 1208.
24 S. A. Safran, N. Gov, A. Nicolas, U. S. Schwarz and T. Tlusty, *Physica A*, 2005, **352**, 171.
25 F. Huber and J. Käs, *Cytoskeleton*, 2011, **68**, 259.
26 Y. Tseng, T. P. Kole, J. S. H. Lee, E. Fedorov, S. C. Almo, B. W. Schafer and D. Wirtz, *Biochem. Biophys. Res. Commun.*, 2005, **334**, 183.
27 G. G. Borisy and T. M. Svitkina, *Curr. Opin. Cell Biol.*, 2000, **12**, 104.
28 T. J. Mitchison and L. P. Cramer, *Cell*, 1996, **84**, 371.
29 B. Wagner, R. Tharmann, I. Haase, M. Fischer and A. R. Bausch, *Proc. Natl. Acad. Sci. U. S. A.*, 2006, **103**, 13974.
30 P. A. Janmey, S. Hvidt, J. Lamb and T. P. Stossel, *Nature*, 1990, **345**, 89.
31 M. L. Gardel, J. H. Shin, F. C. MacKintosh, L. Mahadevan, P. Matsudeira and D. A. Weitz, *Science*, 2004, **304**, 1301.
32 J. H. Shin, M. L. Gardel, L. Mahadevan, P. Matsudaira and D. A. Weitz, *Proc. Natl. Acad. Sci. U. S. A.*, 2004, **101**, 9636.
33 M. L. Gardel, F. Nakamura, J. H. Hartwig, J. C. Crocker, T. P. Stossel and D. A. Weitz, *Proc. Natl. Acad. Sci. U. S. A.*, 2006, **103**, 1762.
34 O. Lieleg, K. M. Schmoller, C. J. Cyron, Y. Luan, W. A. Wall and A. R. Bausch, *Soft Matter*, 2009, **5**, 1796.
35 A. R. Bausch and K. Kroy, *Nat. Phys.*, 2006, **2**, 231.
36 D. A. Head, G. Gompper and W. J. Briels, *Soft Matter*, 2011, **7**, 3116.
37 G. A. Buxton, N. Clarke and P. J. Hussey, *eXPRESS Polym. Lett.*, 2009, **3**, 579.
38 P. Chen and V. B. Shenoy, *Soft Matter*, 2011, **7**, 355.
39 L. T. Nguyen, W. Yang, Q. Wang and L. S. Hirst, *Soft Matter*, 2009, **5**, 2033.
40 L. T. Nguyen and L. S. Hirst, *Phys. Rev. E: Stat., Nonlinear, Soft Matter Phys.*, 2011, **83**, 031910.
41 O. Pelletier, E. Pokidysheva, L. S. Hirst, N. Bouxsein, Y. Li and C. R. Safinya, *Phys. Rev. Lett.*, 2003, **91**, 148102.
42 R. Chelakkot, R. Lipowsky and T. Gruhn, *Soft Matter*, 2009, **5**, 1504.
43 T. Kim, W. Hwang and R. D. Kamm, *Exp. Mech.*, 2009, **49**, 91.
44 J. Kang, R. L. Steward, Y. T. Kim, R. S. Schwartz, P. R. LeDuc and K. M. Puskar, *J. Theor. Biol.*, 2011, **274**, 109.
45 T. Kim, W. Hwang, H. Lee and R. D. Kamm, *J. Comput. Biol.*, 2009, **5**, e1000439.
46 D. A. Head, A. J. Levine and F. C. MacKintosh, *Phys. Rev. Lett.*, 2003, **91**, 108102.
47 E. M. Huisman, T. van Dillen, P. R. Onck and E. Van der Giessen, *Phys. Rev. Lett.*, 2007, **99**, 208103.
48 E. M. Huisman, C. Heussinger, C. Storm and G. T. Barkema, *Phys. Rev. Lett.*, 2010, **105**, 118101.
49 M. Bai, A. R. Missel, A. J. Levine and W. S. Klug, *Acta Biomater.*, 2011, **7**, 2109.
50 M. Bai, A. R. Missel, W. S. Klug and A. J. Levine, *Soft Matter*, 2011, **7**, 907.
51 E. Grazi, *FEBS Lett.*, 1997, **405**, 249.
52 A. Spiros and L. Edelstein-Keshet, *Bull. Math. Biol.*, 1998, **60**, 275.
53 K. E. Kasza, C. P. Broedersz, G. H. Koenderink, Y. C. Lin, W. Messner, E. A. Millman, F. Nakamura, T. P. Stossel, F. C. MacKintosh and D. A. Weitz, *Biophys. J.*, 2010, **99**, 1091.
54 J. Xu, J. F. Casella and T. D. Pollard, *Cell Motil. Cytoskeleton*, 1999, **42**, 73.
55 P. Janmey, Cell Membranes and The Cytoskeleton, in *The Structure and Dynamics of Membranes*, ed. R. Lipowsky and E. Sackmann, Elsevier, Amsterdam, 1995, pp. 805–849.
56 S. X. Sun, S. Walcott and C. W. Wolgemuth, *Curr. Biol.*, 2010, **20**, R649.
57 R. H. Colby, J. R. Gillmor and M. Rubinstein, *Phys. Rev. E: Stat. Phys., Plasmas, Fluids, Relat. Interdiscip. Top.*, 1993, **48**(5), 3712.
58 D. Stauffer and A. Aharony, *Introduction to Percolation Theory*, Taylor and Francis, London, 1st edn, 1992.
59 M. Sahimi, *Applications of Percolation Theory*, Taylor and Francis, London, 1st edn, 1994.
60 Y. Liu and R. B. Pandey, *J. Chem. Phys.*, 1996, **105**(2), 825.
61 J. Brzychczyk, *Phys. Rev. C: Nucl. Phys.*, 2006, **73**(2), 024601.
62 C. Lusignan, T. Mourey, J. Wilson and R. Colby, *Phys. Rev. E: Stat. Phys., Plasmas, Fluids, Relat. Interdiscip. Top.*, 1999, **60**, 5657.
63 P. de Gennes, *J. Phys., Lett.*, 1977, **38**, L355.
64 P. Flory, *J. Am. Chem. Soc.*, 1941, **63**, 3083.
65 P. Flory, *J. Am. Chem. Soc.*, 1941, **63**, 3091.
66 W. Stockmayer, *J. Chem. Phys.*, 1943, **11**, 45.
67 R. H. Colby, J. R. Gillmor and M. Rubinstein, *Macromolecules*, 1992, **25**, 7180.
68 L. Onsager, *Ann. N. Y. Acad. Sci.*, 1949, **51**, 627.
69 D. Frenkel, *J. Phys. Chem.*, 1987, **91**, 4912.
70 C. D. Lorenz and R. M. Ziff, *Phys. Rev. E: Stat. Phys., Plasmas, Fluids, Relat. Interdiscip. Top.*, 1998, **57**, 230.
71 C. D. Lorenz, R. May and R. M. Ziff, *J. Stat. Phys.*, 2000, **98**, 961.
72 V. A. Vyssotsky, S. B. Gordon, H. L. Frisch and J. M. Hammersley, *Phys. Rev.*, 1961, **123**, 1566.